Paper pa 02 - 089
Submitted to the 28th International Conference on High Energy Physics
ICHEP'96, Warsaw, Poland, July 1996

Inclusive D^0 and $D^{*\pm}$ Production in Deep Inelastic ep Scattering at HERA

H1 Collaboration

Abstract

First results on inclusive $\overset{(-)}{D}{}^0$ and $D^{*\pm}$ production in deep inelastic ep scattering are reported using data collected by the H1 experiment at HERA in 1994. Differential cross sections are presented for both channels and are found to agree well with QCD predictions based on the boson gluon fusion process. A charm production cross section for 10 GeV$^2 \leq Q^2 \leq 100$ GeV^2 and $0.01 \leq y \leq 0.7$ of $\sigma(ep \rightarrow c\bar{c}X) = (17.4 \pm 1.6 \pm 1.7 \pm 1.4)$ nb is derived. A first measurement of the charm contribution $F_2^{c\bar{c}}(x, Q^2)$ to the proton structure function for Bjorken x between $8 \cdot 10^{-4}$ and $8 \cdot 10^{-3}$ is presented. In this kinematic range a ratio $F_2^{c\bar{c}}/F_2 = 0.237 \pm 0.021^{+0.043}_{-0.039}$ is observed.

Dedicated to Hans Duhm

C. Adloff[35], S. Aid[13], M. Anderson[23], V. Andreev[26], B. Andrieu[29], R.-D. Appuhn[11], C. Arndt[11], A. Babaev[25], J. Bähr[37], J. Bán[18], Y. Ban[28], P. Baranov[26], E. Barrelet[30], R. Barschke[11], W. Bartel[11], M. Barth[4], U. Bassler[30], H.P. Beck[39], H.-J. Behrend[11], A. Belousov[26], Ch. Berger[1], G. Bernardi[30], G. Bertrand-Coremans[4], M. Besançon[9], R. Beyer[11], P. Biddulph[23], P. Bispham[23], J.C. Bizot[28], V. Blobel[13], K. Borras[8], F. Botterweck[4], V. Boudry[29], A. Braemer[15], W. Braunschweig[1], V. Brisson[28], P. Bruel[29], D. Bruncko[18], C. Brune[16], R. Buchholz[11], L. Büngener[13], J. Bürger[11], F.W. Büsser[13], A. Buniatian[4,40], S. Burke[19], M.J. Burton[23], D. Calvet[24], A.J. Campbell[11], T. Carli[27], M. Charlet[11], D. Clarke[5], A.B. Clegg[19], B. Clerbaux[4], S. Cocks[20], J.G. Contreras[8], C. Cormack[20], J.A. Coughlan[5], A. Courau[28], M.-C. Cousinou[24], G. Cozzika[9], L. Criegee[11], D.G. Cussans[5], J. Cvach[31], S. Dagoret[30], J.B. Dainton[20], W.D. Dau[17], K. Daum[36], M. David[9], C.L. Davis[19], B. Delcourt[28], A. De Roeck[11], E.A. De Wolf[4], M. Dirkmann[8], P. Dixon[19], P. Di Nezza[33], W. Dlugosz[7], C. Dollfus[39], J.D. Dowell[3], H.B. Dreis[2], A. Droutskoi[25], O. Dünger[13], H. Duhm[12,†], J. Ebert[35], T.R. Ebert[20], G. Eckerlin[11], V. Efremenko[25], S. Egli[39], R. Eichler[38], F. Eisele[15], E. Eisenhandler[21], E. Elsen[11], M. Erdmann[15], W. Erdmann[37], E. Evrard[4], A.B. Fahr[13], L. Favart[28], A. Fedotov[25], D. Feeken[13], R. Felst[11], J. Feltesse[9], J. Ferencei[18], F. Ferrarotto[33], K. Flamm[11], M. Fleischer[8], M. Flieser[27], G. Flügge[2], A. Fomenko[26], B. Fominykh[25], J. Formánek[32], J.M. Foster[23], G. Franke[11], E. Fretwurst[12], E. Gabathuler[20], K. Gabathuler[34], F. Gaede[27], J. Garvey[3], J. Gayler[11], M. Gebauer[37], H. Genzel[1], R. Gerhards[11], A. Glazov[37], U. Goerlach[11], L. Goerlich[6], N. Gogitidze[26], M. Goldberg[30], D. Goldner[8], K. Golec-Biernat[6], B. Gonzalez-Pineiro[30], I. Gorelov[25], C. Grab[38], H. Grässler[2], T. Greenshaw[20], R.K. Griffiths[21], G. Grindhammer[27], A. Gruber[27], C. Gruber[17], J. Haack[37], T. Hadig[1], D. Haidt[11], L. Hajduk[6], M. Hampel[1], W.J. Haynes[5], G. Heinzelmann[13], R.C.W. Henderson[19], H. Henschel[37], I. Herynek[31], M.F. Hess[27], K. Hewitt[3], W. Hildesheim[11], K.H. Hiller[37], C.D. Hilton[23], J. Hladký[31], K.C. Hoeger[23], M. Höppner[8], D. Hoffmann[11], T. Holtom[20], R. Horisberger[34], V.L. Hudgson[3], M. Hütte[8], M. Ibbotson[23], H. Itterbeck[1], A. Jacholkowska[28], C. Jacobsson[22], M. Jaffre[28], J. Janoth[16], T. Jansen[11], L. Jönsson[22], D.P. Johnson[4], H. Jung[9], P.I.P. Kalmus[21], M. Kander[11], D. Kant[21], R. Kaschowitz[2], U. Kathage[17], J. Katzy[15], H.H. Kaufmann[37], O. Kaufmann[15], M. Kausch[11], S. Kazarian[11], I.R. Kenyon[3], S. Kermiche[24], C. Keuker[1], C. Kiesling[27], M. Klein[37], C. Kleinwort[11], G. Knies[11], T. Köhler[1], J.H. Köhne[27], H. Kolanoski[37,42], F. Kole[7], S.D. Kolya[23], V. Korbel[11], M. Korn[8], P. Kostka[37], S.K. Kotelnikov[26], T. Krämerkämper[8], M.W. Krasny[6,30], H. Krehbiel[11], D. Krücker[27], A. Küpper[35], H. Küster[22], M. Kuhlen[27], T. Kurča[37], J. Kurzhöfer[8], D. Lacour[30], B. Laforge[9], R. Lander[7], M.P.J. Landon[21], W. Lange[37], U. Langenegger[38], J.-F. Laporte[9], A. Lebedev[26], F. Lehner[11], S. Levonian[29], G. Lindström[12], M. Lindstroem[22], J. Link[7], F. Linsel[11], J. Lipinski[13], B. List[11], G. Lobo[28], P. Loch[11], J.W. Lomas[23], G.C. Lopez[12], V. Lubimov[25], D. Lüke[8,11], N. Magnussen[35], E. Malinovski[26], S. Mani[7], R. Maraček[18], P. Marage[4], J. Marks[24], R. Marshall[23], J. Martens[35], G. Martin[13], R. Martin[20], H.-U. Martyn[1], J. Martyniak[6], T. Mavroidis[21], S.J. Maxfield[20], S.J. McMahon[20], A. Mehta[5], K. Meier[16], A. Meyer[11], A. Meyer[13], H. Meyer[35], J. Meyer[11], P.-O. Meyer[2], A. Migliori[29], S. Mikocki[6], D. Milstead[20], J. Moeck[27], F. Moreau[29], J.V. Morris[5], E. Mroczko[6], D. Müller[39], G. Müller[11], K. Müller[11], P. Murín[18], V. Nagovizin[25], R. Nahnhauer[37], B. Naroska[13], Th. Naumann[37], I. Négri[24], P.R. Newman[3], D. Newton[19], H.K. Nguyen[30], T.C. Nicholls[3], F. Niebergall[13], C. Niebuhr[11], Ch. Niedzballa[1], H. Niggli[38], R. Nisius[1], G. Nowak[6], G.W. Noyes[5], M. Nyberg-Werther[22], M. Oakden[20], H. Oberlack[27], J.E. Olsson[11], D. Ozerov[25], P. Palmen[2], E. Panaro[11], A. Panitch[4], C. Pascaud[28], G.D. Patel[20], H. Pawletta[2], E. Peppel[37], E. Perez[9], J.P. Phillips[20], A. Pieuchot[24], D. Pitzl[38], G. Pope[7], S. Prell[11], K. Rabbertz[1], G. Rädel[11], P. Reimer[31], S. Reinshagen[11], H. Rick[8], V. Riech[12], J. Riedlberger[38], F. Riepenhausen[2], S. Riess[13], E. Rizvi[21], S.M. Robertson[3], P. Robmann[39], H.E. Roloff[37,†], R. Roosen[4], K. Rosenbauer[1], A. Rostovtsev[25], F. Rouse[7], C. Royon[9], K. Rüter[27], S. Rusakov[26], K. Rybicki[6], D.P.C. Sankey[5], P. Schacht[27], S. Schiek[13], S. Schleif[16], P. Schleper[15], W. von Schlippe[21], D. Schmidt[35], G. Schmidt[13], A. Schöning[11], V. Schröder[11], E. Schuhmann[27], B. Schwab[15], F. Sefkow[39], M. Seidel[12], R. Sell[11], A. Semenov[25], V. Shekelyan[11], I. Sheviakov[26], L.N. Shtarkov[26], G. Siegmon[17], U. Siewert[17], Y. Sirois[29], I.O. Skillicorn[10], P. Smirnov[26], J.R. Smith[7], V. Solochenko[25], Y. Soloviev[26], A. Specka[29], J. Spiekermann[8], S. Spielman[29], H. Spitzer[13], F. Squinabol[28], M. Steenbock[13], P. Steffen[11], R. Steinberg[2], H. Steiner[11,41], J. Steinhart[13], B. Stella[33], A. Stellberger[16], J. Stier[11], J. Stiewe[16], U. Stößlein[37], K. Stolze[37], U. Straumann[15], W. Struczinski[2], J.P. Sutton[3], S. Tapprogge[16], M. Taševský[32], V. Tchernyshov[25], S. Tchetchelnitski[25], J. Theissen[2], C. Thiebaux[29], G. Thompson[21], P. Truöl[39], K. Tzamariudaki[11], G. Tsipolitis[38], J. Turnau[6], J. Tutas[15], P. Uelkes[2], A. Usik[26], S. Valkár[32], A. Valkárová[32], C. Vallée[24], D. Vandenplas[29], P. Van Esch[4], P. Van Mechelen[4], Y. Vazdik[26], P. Verrecchia[9], G. Villet[9], K. Wacker[8], A. Wagener[2], M. Wagener[34], A. Walther[8], B. Waugh[23], G. Weber[13], M. Weber[16], D. Wegener[8], A. Wegner[27], T. Wengler[15], M. Werner[15], L.R. West[3], S. Wiesand[35] T. Wilksen[11], S. Willard[7], M. Winde[37], G.-G. Winter[11], C. Wittek[13], M. Wobisch[2], E. Wünsch[11], J. Žáček[32], D. Zarbock[12], Z. Zhang[28], A. Zhokin[25], P. Zini[30], F. Zomer[28], J. Zsembery[9], K. Zuber[16], and M. zurNedden[39]

[1] *I. Physikalisches Institut der RWTH, Aachen, Germany*[a]
[2] *III. Physikalisches Institut der RWTH, Aachen, Germany*[a]
[3] *School of Physics and Space Research, University of Birmingham, Birmingham, UK*[b]
[4] *Inter-University Institute for High Energies ULB-VUB, Brussels; Universitaire Instelling Antwerpen, Wilrijk; Belgium*[c]
[5] *Rutherford Appleton Laboratory, Chilton, Didcot, UK*[b]
[6] *Institute for Nuclear Physics, Cracow, Poland*[d]
[7] *Physics Department and IIRPA, University of California, Davis, California, USA*[e]
[8] *Institut für Physik, Universität Dortmund, Dortmund, Germany*[a]
[9] *CEA, DSM/DAPNIA, CE-Saclay, Gif-sur-Yvette, France*
[10] *Department of Physics and Astronomy, University of Glasgow, Glasgow, UK*[b]
[11] *DESY, Hamburg, Germany*[a]
[12] *I. Institut für Experimentalphysik, Universität Hamburg, Hamburg, Germany*[a]
[13] *II. Institut für Experimentalphysik, Universität Hamburg, Hamburg, Germany*[a]

[14] *Max-Planck-Institut für Kernphysik, Heidelberg, Germany*[a]
[15] *Physikalisches Institut, Universität Heidelberg, Heidelberg, Germany*[a]
[16] *Institut für Hochenergiephysik, Universität Heidelberg, Heidelberg, Germany*[a]
[17] *Institut für Reine und Angewandte Kernphysik, Universität Kiel, Kiel, Germany*[a]
[18] *Institute of Experimental Physics, Slovak Academy of Sciences, Košice, Slovak Republic*[f]
[19] *School of Physics and Chemistry, University of Lancaster, Lancaster, UK*[b]
[20] *Department of Physics, University of Liverpool, Liverpool, UK*[b]
[21] *Queen Mary and Westfield College, London, UK*[b]
[22] *Physics Department, University of Lund, Lund, Sweden*[g]
[23] *Physics Department, University of Manchester, Manchester, UK*[b]
[24] *CPPM, Université d'Aix-Marseille II, IN2P3-CNRS, Marseille, France*
[25] *Institute for Theoretical and Experimental Physics, Moscow, Russia*
[26] *Lebedev Physical Institute, Moscow, Russia*[f]
[27] *Max-Planck-Institut für Physik, München, Germany*[a]
[28] *LAL, Université de Paris-Sud, IN2P3-CNRS, Orsay, France*
[29] *LPNHE, Ecole Polytechnique, IN2P3-CNRS, Palaiseau, France*
[30] *LPNHE, Universités Paris VI and VII, IN2P3-CNRS, Paris, France*
[31] *Institute of Physics, Czech Academy of Sciences, Praha, Czech Republic*[f,h]
[32] *Nuclear Center, Charles University, Praha, Czech Republic*[f,h]
[33] *INFN Roma 1 and Dipartimento di Fisica, Università Roma 3, Roma, Italy*
[34] *Paul Scherrer Institut, Villigen, Switzerland*
[35] *Fachbereich Physik, Bergische Universität Gesamthochschule Wuppertal, Wuppertal, Germany*[a]
[36] *Rechenzentrum, Bergische Universität Gesamthochschule Wuppertal, Wuppertal, Germany*
[37] *DESY, Institut für Hochenergiephysik, Zeuthen, Germany*[a]
[38] *Institut für Teilchenphysik, ETH, Zürich, Switzerland*[i]
[39] *Physik-Institut der Universität Zürich, Zürich, Switzerland*[i]
[40] *Visitor from Yerevan Phys. Inst., Armenia*
[41] *On leave from LBL, Berkeley, USA*
[42] *Institut für Physik, Humboldt-Universität, Berlin, Germany*[a]
† *Deceased*

[a] *Supported by the Bundesministerium für Bildung, Wissenschaft, Forschung und Technologie, FRG, under contract numbers 6AC17P, 6AC47P, 6DO57I, 6HH17P, 6HH27I, 6HD17I, 6HD27I, 6KI17P, 6MP17I, and 6WT87P*
[b] *Supported by the UK Particle Physics and Astronomy Research Council, and formerly by the UK Science and Engineering Research Council*
[c] *Supported by FNRS-NFWO, IISN-IIKW*
[d] *Supported by the Polish State Committee for Scientific Research, grant nos. 115/E-743/SPUB/P03/109/95 and 2 P03B 244 08p01, and Stiftung für Deutsch-Polnische Zusammenarbeit, project no.506/92*
[e] *Supported in part by USDOE grant DE F603 91ER40674*
[f] *Supported by the Deutsche Forschungsgemeinschaft*

[g] *Supported by the Swedish Natural Science Research Council*
[h] *Supported by GA ČR, grant no. 202/93/2423, GA AV ČR, grant no. 19095 and GA UK, grant no. 342*
[i] *Supported by the Swiss National Science Foundation*

1 Introduction

The measurement of the charm production cross section in deep inelastic lepton nucleon scattering (DIS) is of importance for the understanding of the parton densities in the nucleon [1]. To order $\alpha\alpha_s$ deep inelastic electron nucleon scattering proceeds via the generic diagrams depicted in Fig. 1. There is some evidence from the EMC collaboration [2], that heavy quark production should be dominated by the *boson gluon fusion* process (Fig. 1c),

$$\gamma(Z^0)g \rightarrow c\bar{c}, \tag{1}$$

which has been calculated in next to leading order [3]. Charm sea quark contributions (Fig. 1a,b), where only a single (anti)charm quark is recoiling against the proton, should contribute only to a small extent. Charm production due to fragmentation is suppressed by heavy quark mass effects and is therefore expected to be small [4]. For the e^+e^- annihilation process this expectation has been confirmed by recent measurements on the Z^0 resonance [5, 6]. Charmed hadron production via the decay of b flavored hadrons is negligible at HERA, because of the small b production cross section. The intrinsic

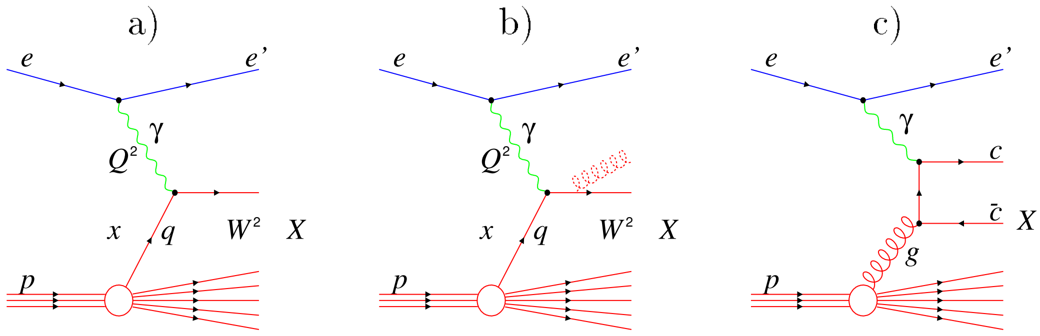

Figure 1: Generic Feynman diagrams for deep inelastic ep scattering up to order $\alpha\alpha_s$: (a) ep interaction of the virtual probe (γ, Z^0) with a valence or a sea quark in the proton according to the quark parton model (QPM), (b) corrections to process (a) due to gluon radiation off the struck quark before or after interacting with the probe (QCD Compton scattering, QCDC), and (c) contribution due to boson gluon fusion (BGF).

charm model [7], where the proton wave function fluctuates to a $|uudc\bar{c}\rangle$ state at the level of a few permille, will give rise to charm production at large Bjorken x. Currently the detection of this process is beyond the scope of HERA experiments.

A measurement of the charm contribution $F_2^{c\bar{c}}(x, Q^2)$ to the structure function of the proton is supposed to provide information on the nature of the charm production process. Present parton density calculations may include heavy flavors in the proton via two different routes. One is to include charm in the massless quark evolution [8] starting with a charm density of zero at a scale Q_0^2 of the momentum transfer squared of the virtual photon, which depends on the mass of the charm quark. The second produces charm exclusively via boson gluon fusion taking into account the charm quark mass [9]. This effective proceedure is presently used in ref. [10, 11, 12]. Although both approaches may lead to very similar predictions for $F_2^{c\bar{c}}(x, Q^2)$, the resulting charm quark momentum spectra will differ. Therefore the momentum distribution of the charmed hadrons allows a sensitive test of the charm production mechanism.

If the photon gluon fusion process is the dominant source of charmed hadrons in deep inelastic ep scattering, the observation of inclusive charmed hadrons production represents a sensitive probe of the gluon density $xg(x,Q^2)$ in the proton. The measurement of $F_2^{c\bar{c}}(x,Q^2)$ can then be used to test different parton density parameterizations.

In this paper a study of inclusive $\overset{(-)}{D}{}^0$ and $D^{*\pm}$ production via the decay channels

$$D^0 \rightarrow K^-\pi^+ \tag{2}$$

and

$$D^{*+} \rightarrow D^0\pi^+ \rightarrow K^-\pi^+\pi^+ \tag{3}$$

is presented[1]. After a brief description of the components of the H1 detector relevant to this analysis (sec. 2) the kinematics of inclusive ep scattering is introduced (sec. 3). The Monte Carlo simulations used to determine the D meson detection efficiencies and to correct the data are briefly described thereafter (sec. 4). The selection of deep inelastic charm events and the possible contributions of background sources are then discussed (sec. 5). The measured D^0 and D^{*+} integrated and differential cross sections are presented in sec. 6 and compared with QCD based model predictions for heavy flavor production in deep inelastic ep scattering. Charm production at HERA is also compared with data from νN scattering. The charm contribution, $F_2^{c\bar{c}}(x,Q^2)$, to the proton structure function is discussed. Finally, the results are summarized in sec. 7.

2 H1 Detector and Data Sample

In 1994 HERA has been operated with 820 GeV protons colliding with 27.6 GeV electrons and positrons[2]. The H1 detector [13] is a nearly hermetic multi-purpose apparatus built to investigate the inelastic high-energy interactions of electrons and protons at HERA. Closest to the interaction point are the central and forward[3] (FT) tracking systems, which are surrounded by a liquid argon calorimeter consisting of an electromagnetic and a hadronic section. A super-conducting solenoid surrounding both the tracking system and the calorimeter provides a uniform magnetic field of 1.15 T parallel to the beam line. The outermost detector component, the instrumented iron, allows the measurement of the hadronic energy leaking out of the calorimeter, as well as the identification of muon tracks.

The analysis presented in this paper relies essentially on parts of the central tracking system and on the backward electromagnetic calorimeter (BEMC) which are described briefly in the following.

The central jet chamber (CJC) consists of two concentric drift chambers covering a polar angle of $15° \leq \Theta \leq 165°$. It is supplemented by two cylindrical drift chambers

[1]Henceforth, charge conjugate states are always implicitly included.
[2]Subsequently electrons will denote both, electrons and positrons, respectively.
[3]The positive z axis of the H1 coordinate system is defined by the proton beam direction.

at radii of 18 and 47 cm to determine the z coordinate of the tracks. A cylindrical proportional chamber is attached to each of the z drift chambers for triggering.

In the backward region, the polar angle acceptance of the multi-wire proportional chamber (BPC) covers the range $155^o \leq \Theta \leq 174.5^o$. The reconstructed space point together with the z vertex position of the event defines the polar angle of the scattered electron with a resolution of 1 mrad.

The BPC is attached to the BEMC, which covers the polar angular region of $155^o < \Theta < 176^o$. An energy resolution of $\sigma(E)/E \approx 0.1/\sqrt{E/\mathrm{GeV}} \oplus 0.42\mathrm{GeV}/E \oplus 0.03$ is obtained. The energy calibration is known to an accuracy of 1% [14]. A scintillator hodoscope (TOF) situated behind the BEMC is used to veto proton induced background events based on their early time of arrival compared with particles from the interaction at the nominal ep vertex.

This analysis is restricted to DIS events which have a scattered electron in the backward region. These events were triggered by an electromagnetic shower in the BEMC with an energy in excess of 4 GeV which was not vetoed by an out of time signal in the TOF. The trigger efficiency has been determined from the data using the redundancy of the H1 trigger system. For energies of the scattered electron candidate $E_e' > 13$ GeV, the trigger efficiency is 100%.

The luminosity is determined from the rate of the Bethe-Heitler reaction $ep \to ep\gamma$. The analysis presented in this paper is based on data taken during 1994 running periods with electron and positron beams and corresponds to a total integrated luminosity of $\mathcal{L}_{int} = 2.97$ pb^{-1}, with an overall uncertainty of 1.5% [15].

3 Kinematics

At fixed center of mass energy, $\sqrt{s}$, the kinematics of the inclusive scattering process $ep \to eX$ is completely determined by two independent Lorentz invariant variables, which may be any two of the Bjorken scaling variables x and y, the momentum squared Q^2 of the virtual boson and the invariant mass squared W^2 of the hadronic final state. In this analysis these variables are determined from the measurement of the energy E_e' and the polar angle Θ_e of the scattered electron according to the expressions (where the electron and proton masses are neglected)

$$\begin{aligned} Q^2 &= 4E_eE_e'\cos^2\left(\frac{\Theta_e}{2}\right) & y &= 1 - \frac{E_e'}{E_e}\sin^2\left(\frac{\Theta_e}{2}\right) \\ x &= \frac{Q^2}{ys} & W^2 &= Q^2\left(\frac{1-x}{x}\right) \end{aligned} \tag{4}$$

where $s = 4E_eE_p$, and E_e and E_p denote the energies of the incoming electron and proton, respectively. Here the scattering angle Θ_e is defined with respect to the proton beam direction.

4 Monte Carlo Simulation

Monte Carlo simulation programs are used in order to correct the data and to estimate the systematic uncertainties associated with the measurement. For the determination of the acceptance of the detector and the D^0 and D^{*+} selection efficiencies, heavy flavor (charm and bottom) DIS events are generated using the AROMA 2.1 [16] program. This simulates neutral current heavy quark production via the boson gluon fusion process, which is implemented in leading order QCD including heavy quark mass effects. A charm quark mass of $m_c = 1.5$ GeV is used. Higher order QCD radiation includes initial and final state parton showers (PS) [17] using the LEPTO 6.1 code [18]. JETSET 7.4 [19] is used to perform the hadronization according to the Lund string model with the symmetric Lund fragmentation function [20]. For the gluon density in the proton the MRSH parameterization [11] is used. This is compatible with measurements of the proton structure function at HERA [21]. In order to test the sensitivity of the results to the charm quark mass heavy flavor DIS events are also generated with $m_c = 1.3$ GeV and $m_c = 1.7$ GeV.

For the study of any charm contribution to the proton sea, heavy flavor events are also generated using the LEPTO 6.1 program [18]. In this generator heavy quark mass effects are not included. To avoid the divergences in the QCD matrix elements, a cut in the smallest invariant mass m_{ij} of any two partons of an event is introduced. The difference in the cross section, obtained with this cut, to the total DIS cross section is then attributed to sea quarks in the proton, thus also generating QPM type charm events, where a single charm quark recoils against the proton remnant.

5 Event Selection

5.1 Selection of Deep Inelastic Scattering Events

For the selection of deep inelastic ep interactions the electron candidate is identified as the particle giving in the BEMC the most energetic cluster, which has also to fulfill the following conditions : (a) its center of gravity has a radial distance of less than 4 cm from a reconstructed BPC point, and (b) its lateral shower size has to be smaller than 4 cm. In order to calculate the kinematic variables precisely the position of the event vertex is needed. It is defined by at least one well measured track crossing the beam axis.

The basic kinematic constraints are that the electron polar angle is in the range $155^o \leq \Theta_e \leq 173^o$ and that the electron energy $E_e' > 13$ GeV. The latter requirement ensures that the trigger is fully efficient and the photoproduction background is small [15]. The analysis is thus restricted to 10 GeV$^2 < \mathrm{Q}^2 < 100$ GeV^2 and $y < 0.53$.

The dominant source of non-ep background in the event sample is due to interactions of the proton beam with the residual gas and the beam collimators before the H1 detector. The level of this background is studied with events originating from proton bunches having no colliding electron bunch partner. It is found to be less than 0.25%

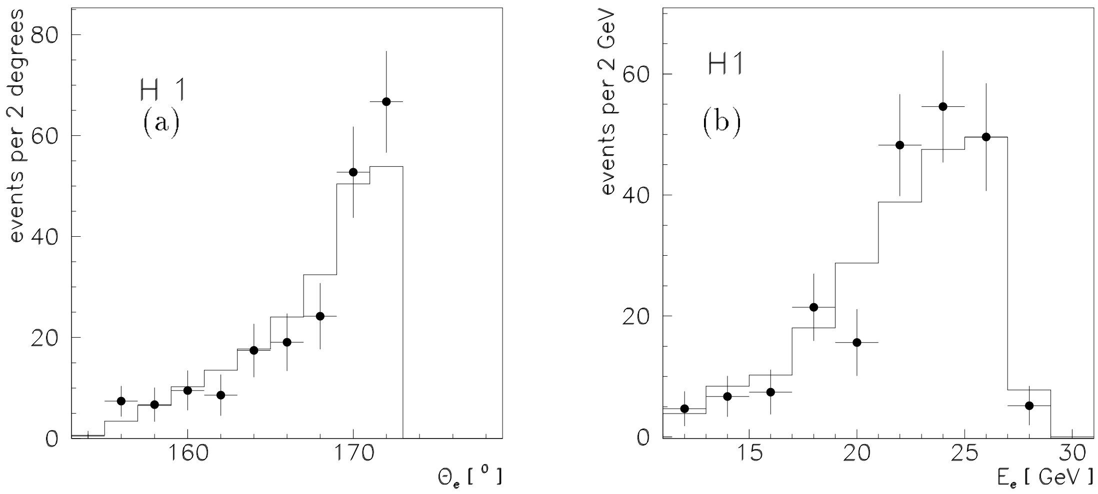

Figure 2: Distribution of (a) the polar angle and (b) the energy of the scattered electron for charm events as observed in the D^{*+} analysis. The background subtracted data is compared with the expectation of the AROMA (histogram) Monte Carlo simulation, normalized to the number of events in the data. Only statistical errors are shown.

of the total number of the selected events.

Events originating from photoproduction, in which the scattered electron escapes detection but hadronic activity in the BEMC fakes an electron, are the only significant ep related background. On the basis of Monte Carlo simulations, using the PYTHIA generator [19], this background is found to be less than 0.4%.

Figure 2 shows the distribution of the angle and the energy of the scattered electron for charm events as selected by the D^{*+} analysis in comparison to the expectation of the AROMA Monte Carlo simulation. Good agreement is observed between the background subtracted data and the simulation.

5.2 Selection of Charm Events

Reconstructed $D^0(1864)$ and $D^{*+}(2010)$ mesons are used to tag heavy quark production. The analysis is based on charged particles reconstructed in the CJC. Apart from the electron candidate at least 2 or 3 tracks, depending on the decay mode, have to be fitted to a common event vertex. No particle identification is applied so each track may be assumed to be a pion or a kaon. A minimum track length of 10 cm in the plane perpendicular to the beam direction is required for those tracks considered to form the D^0 candidate. In both analyses the $K^-\pi^+$ mass combination has to lie within the interval $|\eta_{K\pi}| \leq 1.5$, where $\eta = -\ln\tan\Theta/2$ denotes the pseudorapidity.

The D^0 is identified via its decay mode

$$D^0 \rightarrow K^-\pi^+ \tag{5}$$

and the D^{*+} through the decay chain

$$D^{*+} \to D^0 \pi^+_{slow} \to K^- \pi^+ \pi^+_{slow} \,. \tag{6}$$

For the latter use is made of the tight kinematic constraint for the decay of $D^{*+} \to D^0 \pi^+_{slow}$ [22]. A better resolution is expected for the mass difference

$$\Delta m = m(D^0 \pi^+_{slow}) - m(D^0) \tag{7}$$

than for the D^{*+} mass itself, the width of which is dominated by the momentum resolution of the detector. No cut on the track length is applied in selecting the slow pion.

In addition to the reconstruction of the specific final states the general strategy in searching for charm induced events is based on the hard fragmentation of charmed hadrons [23]. The analysis is performed in the hadronic center of mass ($\gamma^* p$) system. In analogy to the analyses performed by e^+e^- experiments the quantity

$$x_D = \left(\frac{|\vec{p}^{\,*}_{D^0}|}{|\vec{p}^{\,*}_{p}|} \right) = \frac{2\,|\vec{p}^{\,*}_{D^0}|}{W} \tag{8}$$

is defined for the D^0 in the $\gamma^* p$ frame for both decay channels[4]. The mean $\langle x_D \rangle$ of particle combinations originating from D^0 mesons is found to be significantly larger than for the combinatorial background. It therefore may be expected that the D^0 decay products have large momenta in the $\gamma^* p$ system, especially in view of the low multiplicity of the decay mode used in this analysis. In order to take advantage of this fact a ranking of the charged particles is introduced, such that the particle of a given charge having the largest momentum in the $\gamma^* p$ system gets the rank $R = 1$, the particle with the second largest momentum gets the rank $R = 2$, etc. Cut are applied in both, the normalized momentum x_D and the rank of the particles in the subsequent analyses in order to suppress the combinatorial background.

5.2.1 Selection of $D^{*+} \to D^0 \pi^+_{slow} \to K^- \pi^+ \pi^+_{slow}$ Decays

Only particles having a transverse momentum of $p_t > 0.25$ GeV in the laboratory frame are considered for the reconstruction of D^0 candidates. The mass combinations $m_{K\pi}$ fulfilling the requirements

$$(R_K = 1 \wedge R_\pi \leq 3) \vee (R_\pi = 1 \wedge R_K \leq 2) \tag{9}$$

are calculated for each event. The asymmetric cut in the order of the kaon (R_K) and the pion (R_π) accounts for the effect of their different masses. The fractional momentum of the mass combinations has to satisfy $x_D > 0.25$. At small Bjorken x large x_D favors D^0 candidates going backward in the laboratory frame. Also those $m_{K\pi}$ mass combinations are accepted, which satisfy the condition $p_t(K^-\pi^+) > 3$ GeV, irrespectively of R_K, R_π and x_D, to retain the D^{*+} mesons going in the forward direction at small Bjorken x. The $m_{K\pi}$ combinations within ± 90 MeV of the nominal D^0 mass of 1.865 GeV are

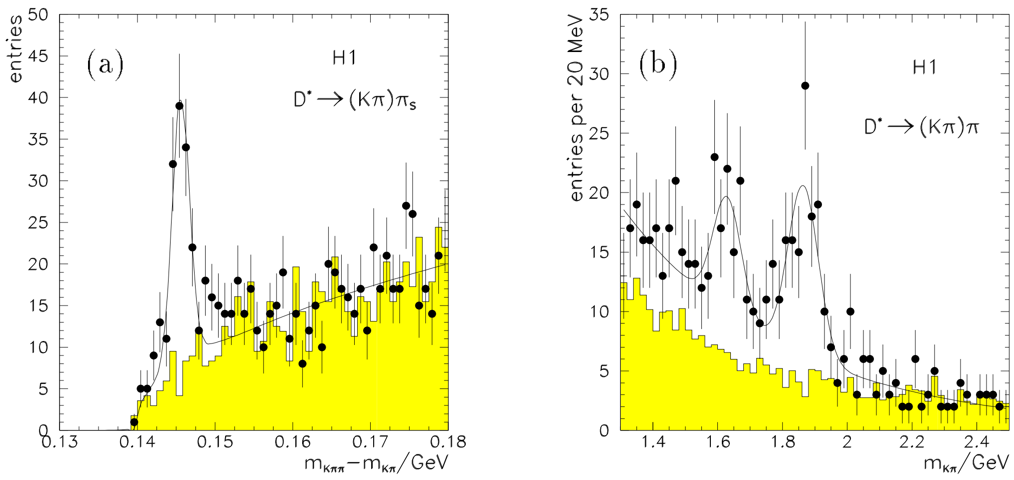

Figure 3: Distribution of (a) the mass difference Δm and (b) the $K^-\pi^+$ mass for DIS events selected as described in the text. The data points in (a) are obtained from the $K^-\pi^+$ mass combinations fulfilling $|m_{K\pi} - m_{D^0}| \leq 90$ MeV. The shaded histogram shows the background expectation, which is obtained from the high mass sideband $2.05\ \mathrm{GeV} \leq \mathrm{m_{K\pi}} \leq 2.5\ \mathrm{GeV}$ normalized to the region $0.160\ \mathrm{GeV} \leq \Delta\mathrm{m} \leq 0.180\ \mathrm{GeV}$. The data points in (b) are obtained from the candidates in an interval of 2.2 MeV around the nominal Δm value expected for the decay $D^{*+} \rightarrow D^0\pi^+$. The shaded histogram shows the background expectation from the region $0.170\ \mathrm{GeV} \leq \Delta\mathrm{m} \leq 0.180\ \mathrm{GeV}$ normalized by the two body phase space factors according to the Δm intervals. The solid lines represent the result of the fits as described in the text.

combined with each additional charged track with $p_t \geq 0.12$ GeV and a charge opposite to that of the kaon candidate.

Figure 3a shows the distribution of the mass difference for accepted $K^-\pi^+\pi^+$ combinations, fulfilling the requirement $|m_{K\pi} - m_{D^0}| \leq 90$ MeV. Clear evidence for D^{*+} production is seen in the signal region, defined by a ± 2.2 MeV window around the expected mass difference of $m_{D^{*+}} - m_{D^0} = 145.4$ MeV. The fit to the data includes the D^{*+} signal, partially reconstructed D^0 mesons and the decay modes $D^0 \rightarrow \pi^+\pi^-$ and $D^0 \rightarrow K^+K^-$, and the two body phase space background. An inclusive D^{*+} yield of 103 ± 13 is observed. The peak position at $\Delta m = 145.5 \pm 0.15$ MeV as well as the width of the Gaussian of $\sigma = (1.04 \pm 0.18)$ MeV agree well with the Monte Carlo expectations. No enhancement is observed in the background sample obtained from mass combinations with $2.05\ \mathrm{GeV} < \mathrm{m_{K\pi}} < 2.5\ \mathrm{GeV}$ as shown by the shaded histogram in Fig. 3[5].

Figure 3b shows the mass distribution of the $K^-\pi^+$ combinations for events in the Δm signal region. The shaded histogram shows the background expectation from the region $0.160\ \mathrm{GeV} \leq \Delta\mathrm{m} \leq 0.180\ \mathrm{GeV}$ scaled by the two body phase space factors. It

[4]Quantities defined in the $\gamma^* p$ system are marked by *.

[5]Since the selection is mainly based on the leading particles in the $\gamma^* p$ frame, the background behavior cannot be studied by using the like sign $K^-\pi^+$ mass combinations.

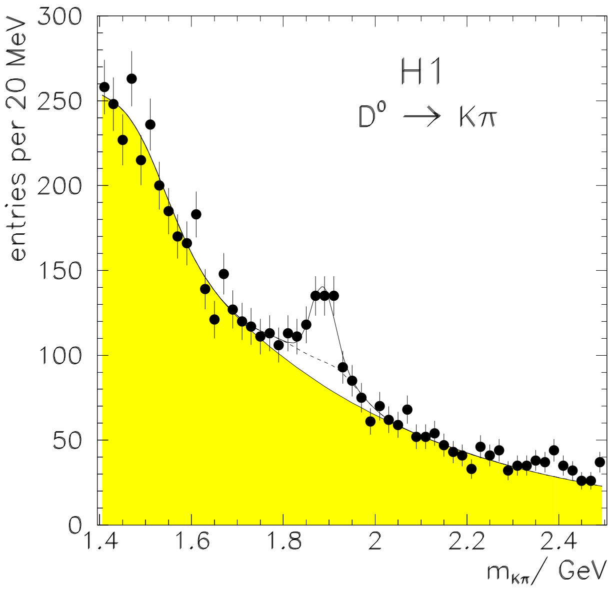

Figure 4: $K^-\pi^+$ mass distribution observed in the inclusive D^0 analysis. The solid line is a fit to the data as indicated in the text. The dashed line shows the contribution from the wrong $K-\pi$ assignment to the tracks. The shaded area indicates contributions to the fit due to combinatorial background and reflections while the dashed line describes the mass distribution for the wrong mass assignment to the tracks.

describes well the $K^-\pi^+$ mass distribution for $m_{K\pi} > 2.05\,\mathrm{GeV}$. Below 2.05 GeVlarge differences are observed in the $m_{K\pi}$ distribution from the D^{*+} signal region as compared to the background expectation. These differences are due to contributions where both particles originate from the decay $D^{*+} \to D^0\pi^+_{slow}$. Clear signals are observed for the decays $D^0 \to K^-\pi^+$ and $D^0 \to K^-\pi^+\pi^0$ where the π^0 is not detected. The fit to the data takes into account these two contributions over an exponentially falling background. The inclusive D^0 yield of 84 ± 16 for the decay $D^0 \to K^-\pi^+$ agrees with the D^{*+} rate obtained from the fit to the Δm distribution.

5.2.2 Selection of $D^0 \to K^-\pi^+$ Decays

For each event the $K^-\pi^+$ mass combination is calculated only for those particles with $p_t \geq 1$ GeV and fulfilling

$$R_K = 1 \wedge R_\pi \leq 2\ . \tag{10}$$

For the $K^-\pi^+$ mass combination a $p_t > 2$ GeV and $x_D > 0.3$ is required. Finally a cut in the helicity angle Θ^*_K of the kaon in the D^0 rest frame with respect to the D^0 direction in the laboratory system of $|\cos\Theta^*_K| < 0.5$ is imposed.

Figure 4 shows the mass distribution of the $K^-\pi^+$ combinations accepted after these cuts. Clear evidence for D^0 production is observed. The fit to the data contains contributions for the D^0 with the correct K, π assignment to the tracks, for the D^0

with the wrong K, π assignment to the tracks, an exponential distribution for the combinatorial background, and contributions due to reflections from other D^0 decay modes and from D^+ decay at small $m_{K\pi}$. An inclusive D^0 signal of 144 ± 19 is observed within the cuts. In total 20 ± 5 events are found to be selected by both the D^0 and D^{*+} analyses.

6 Results

The results on the differential and the integrated cross sections for the production of charmed hadrons in ep collisions are presented for the range 10 GeV$^2 \leq Q^2 \leq 100$ GeV^2 and $0.01 \leq y \leq 0.7$ with a small, 7.8% contribution of the extrapolation from the experimentally accessible range of $y < 0.53$ to 0.7. The cross sections are calculated from the observed numbers N_{obs} of D^0 and D^{*+} candidates, according to

$$\sigma(ep \to DX) = \frac{N_{obs}}{\mathcal{L}_{int} \cdot B \cdot \epsilon_{tot}}, \tag{11}$$

where $\sigma(ep \to DX)$ is used as an abbreviation for both the differential and integral cross sections, respectively. D stands for D^0 and D^{*+} and their charge conjugates. Here $\mathcal{L}_{int}$ and B refer to the integrated luminosity and the branching ratios $B = B(D^0 \to K^-\pi^+) = 0.0401 \pm 0.0014$ and $B = B(D^{*+} \to D^0\pi^+) \cdot B(D^0 \to K^-\pi^+) = 0.0273 \pm 0.0011$ [23]. The quantity ϵ_{tot} is the total efficiency.

The number of observed events, N_{obs}, is obtained from the fits to the spectra. In the case of differential distributions the mass distribution for each bin is fit separately by fixing the position and the width of the signals to those values obtained from the total data sample. The effect of correlations between the detector resolution and the measured quantity is included in the experimental systematic errors. The AROMA Monte Carlo program is used to determine the efficiency arising from the selection procedure and the geometrical acceptance of the detector. A total efficiency, including the acceptance of the apparatus, of $(16.3^{+1.5}_{-2.1})$% and $(5.9^{+0.4}_{-0.6})$% is obtained for the inclusive D^{*+} and the inclusive D^0 analyses, respectively.

The inclusive D^0 and D^{*+} cross sections are then converted into a charm production cross section in deep inelastic ep scattering using the equation

$$\sigma(ep \to ec\bar{c}X) = \frac{1}{2} \cdot \frac{\sigma(ep \to eDX)}{P(c \to D) \cdot (1 + \xi)}, \tag{12}$$

where $P(c \to D)$ denotes the charm quark fragmentation probability into a specific D meson and ξ the correction to apply for charm production via fragmentation or via B meson decays, respectively.

The fragmentation probabilities $P(c \to D^0)$ and $P(c \to D^{*+})$ have to be determined from other experiments. The ARGUS [24] and CLEO [25] results from below the $\Upsilon(4S)$ together with the HRS [26] measurement assuming $P(b \to D^0) = P(c \to D^0)$ are averaged to get $P(c \to D^0) \cdot BR(D^0 \to K^-\pi^+) = 0.0205 \pm 0.0011$. For D^{*+}

	$\sigma(ep \to eDX)$ [nb]	$\sigma(ep \to ec\bar{c}X)$ [nb]
$D^0 \to K^-\pi^+$	$20.4 \pm 2.7^{+2.7}_{-2.4}{}^{+1.6}_{-1.2}$	$19.5 \pm 2.6^{+2.7}_{-2.5}{}^{+1.6}_{-1.2}$
$D^{*+} \to (K^-\pi^+)\pi^+$	$7.8 \pm 1.0^{+1.2}_{-1.0} \pm 0.6$	$15.1 \pm 1.8^{+2.4}_{-2.0} \pm 1.2$
Average		$17.4 \pm 1.6 \pm 1.7 \pm 1.4$

Table 1: Inclusive D meson and charm production cross sections in deep inelastic ep scattering for the kinematic range 10 GeV^2 $<$ Q^2 $<$ 100 GeV^2 and $0.01 < y < 0.7$. The errors refer to the statistical error, the experimental systematic, and the model dependent uncertainties.

mesons the average of all e^+e^- data below the Z^0 leads to $P(c \to D^{*+}) \cdot BR(D^{*+} \to D^0\pi^+) \cdot BR(D^0 \to K^-\pi^+) = 0.0069 \pm 0.0005$ according to the procedure of ref. [5][6].

The main contribution to the correction ξ arises from gluon splitting. Its estimation is based on the OPAL measurement of the mean multiplicity per event for $c\bar{c}$ creation due to gluon splitting with a value $\langle n_{g\to c\bar{c}}\rangle = 0.0238 \pm 0.0048$ [6]. This result has been extrapolated to HERA energies yielding $\xi_{g\to c\bar{c}} = 0.02 \pm 0.02$ for $x_D > 0.25$.

Experiment	ref.	Process	$\frac{\sigma(D^{*\pm}X)}{\sigma(D^0X)}$
H1		$\boldsymbol{ep}$	$\mathbf{0.38 \pm 0.07}$ $\mathbf{\pm 0.06}$
CLEO	[25]	e^+e^-	0.48 ± 0.06
ARGUS	[24]	e^+e^-	0.47 ± 0.06
HRS	[26]	e^+e^-	0.47 ± 0.06
DELPHI	[27]	e^+e^-	0.43 ± 0.05
ALEPH	[28]	e^+e^-	0.36 ± 0.04
NA32	[29]	$\pi\ Si$	0.54 ± 0.05
E769	[30]	$\pi\ Be, Cu, Al, W$	0.39 ± 0.05
		$p\ Be, Cu, Al, W$	0.32 ± 0.13
		$K\ Be, Cu, Al, W$	0.24 ± 0.08

Table 2: Experimental Ratio of the inclusive $D^{*\pm}$ cross section over the inclusive D^0 cross section compared to the results from e^+e^- and hadroproduction experiments.

Model	m_c [GeV]	Predictions [nb]	This Experiment [nb]
GRV	1.5	11.4	17.2 ± 2.3
MRSH	1.3	11.3	17.2 ± 2.3
MRSH	1.5	9.7	17.4 ± 2.3
MRSH	1.7	8.1	16.7 ± 2.2
MRSA′	1.5	9.7	17.4 ± 2.3
MRSD0′	1.5	8.7	18.3 ± 2.4
H1 F_2 fit	1.5	13.6 ± 1.0	17.1 ± 2.3

Table 3: Comparison of predicted charm production cross sections with the present measurement for 10 GeV$^2 \leq$ Q$^2 \leq$ 100 GeV^2 and $0.01 < y < 0.7$. The theoretical predictions are based on NLO calculations [3] for different parton densities and different values of m_c. Also shown is the prediction based on the determination of the gluon density by the H1 NLO fit to the total F_2 data [15]. The experimental cross section is the average from the D^{*+} and D^0 analysis. Total experimental errors are given.

6.1 Integrated Cross Sections

In Tab. 1 the inclusive D meson and charm production cross sections at the Born level are summarized for the kinematic range 10 GeV$^2 <$ Q$^2 <$ 100 GeV^2 and $0.01 < y < 0.7$. Corrections for QED radiations are applied using the HECTOR program [31]. They amount to 5 ± 3 % for the kinematic region explored in this analysis. The errors in Tab. 1 reflect the statistical uncertainties, the experimental systematic and the model dependent uncertainties due to the extrapolation to the full phase space. The experimental systematic errors and the model dependent uncertainties are discussed separately in the subsequent sections. The results of both measurements are in fair agreement. Table 1 also includes the charm production cross section obtained by combining the results of the two analyses.

The ratio on the inclusive D^{*+} over the inclusive D^0 cross section is compared with results from e^+e^- annihilation and hadroproduction experiments in Tab. 2. Agreement is observed with the other experiments[7]. The quoted errors for the present measurement refer to the statistical and the experimental systematic error, and take into account the systematic uncertainties, common to both analyses.

In Tab. 3 the measured charm production cross section is compared to the NLO predictions [3] for different parameterizations of the gluon density in the proton and different values of the charm quark mass m_c. The results from the inclusive D^0 and D^{*+} analyses are combined for the determination of the charm production cross section. The quoted error refers to the total experimental error, which is obtained by adding

[6]The value quoted here differs slightly from that given in [5] because it also includes the measurement of ARGUS [24].

[7]The ratio from the ARGUS and HRS experiment is calculated using a value of $BR(D^{*\pm} \rightarrow D^0\pi^{\pm}) = 0.681$ [23, p. 1171] instead of 0.55 as quoted in their paper [24, 26].

Experimental Systematic Errors	D^0	D^{*+}
reflections, background shape& mass resolution	± 0.10	± 0.11
wrong $K^-\pi^+$ assignment	± 0.03	-
tracker efficiency	${}^{+0.06}_{-0.02}$	${}^{+0.09}_{-0.03}$
luminosity	0.015	0.015
γp contribution	<0.004	<0.004
radiative corrections	± 0.03	± 0.03
branching ratios	± 0.03	± 0.04
total $ep \to eDX$	${}^{+0.13}_{-0.12}$	${}^{+0.15}_{-0.13}$

Table 4: Summary of the relative experimental systematic uncertainties of the integrated inclusive cross section.

the statistical and the experimental systematic errors quadratically. The measured cross section is fairly insensitive to the choice of the model assumptions. For the theoretical predictions, however, the integrated charm production cross section shows strong variations on the model assumptions. All theoretical predictions based on the NLO calculations [3] are below the measured cross section.

The table also includes the comparison of the data with the expectation of the NLO QCD analysis of the structure function data performed by the H1 Collaboration [15]. In the evolution only three light quark flavors are taken into account. Heavy quark contributions are dynamically generated using the BGF prescription given in ref. [32, 33], extended to NLO according to ref. [3]. The scale of the BGF process has been taken as $\sqrt{Q^2+4m_c^2}$ with a charm quark mass of $m_c = 1.5$ GeV. The gluon, sea and valence quark distributions were parameterized at $Q_0^2 = 5$ GeV^2. The QCD parameter Λ_{QCD} is kept fixed to the value of 263 MeV, as determined in ref. [34]. The parton densities are derived from a fit of the evolution equations to the data [15, 35, 36]. The error on the predicted charm production cross section were obtained in propagating the statistical and the uncorrelated experimental systematic errors on the total F_2 data through this fitting procedure [37]. This determination of the gluon density in the proton yields a predicted charm production cross section which comes closer to the result of the current analysis.

6.1.1 Experimental Systematic Uncertainties

The experimental systematic uncertainties are summarized in Tab. 4. By adding the different contributions in quadrature total relative errors of ${}^{+13\%}_{-12\%}$ and ${}^{+15\%}_{-13\%}$ are found for the inclusive D^0 and D^{*+} cross sections, respectively.

Model Uncertainties	D^0	D^{*+}
charm fragmentation function	± 0.04	± 0.04
GRV-HO Gluon	-0.01	-0.01
MRSD0$'$ Gluon	+0.05	+0.05
Gluon from H1 F_2 fit	-0.01	-0.02
$m_c = 1.3$ GeV	± 0.04	+0.03
$m_c = 1.7$ GeV	± 0.04	-0.06
total $ep \to eDX$	${}^{+0.08}_{-0.06}$	± 0.07
fragmentation & gluon splitting	± 0.02	± 0.02
b contribution	<0.02	<0.02
total $ep \to ec\bar{c}X$	${}^{+0.08}_{-0.06}$	± 0.08

Table 5: Summary of the relative model dependent uncertainties of the inclusive D meson and charm production cross sections.

In the case of the inclusive D^0 analysis the dominant experimental systematic uncertainty arises from the description of the combinatorial background and the shape of the reflections below the D^0 mass. A simple phenomenological ansatz has been used to parameterize these contributions in the fit shown in Fig. 4. The uncertainty introduced by this procedure is estimated by varying the $m_{K\pi}$ range in which the data is fitted. The form of the wrong $K - \pi$ assignment and its rate with respect to the correct $K - \pi$ assignment is studied by Monte Carlo simulation. The given error is determined from this simulation.

For the inclusive D^* analysis, the uncertainties coming from the shape of the combinatorial background are determined from the Δm distribution of the high $m_{K\pi}$ sideband, which matches well the two body phase space expectation. The given uncertainty accounts for the fact that the shap of the combinatorial background may differ from the two body phase space prediction. The contribution due to reflections in the D^0 mass window is studied by Monte Carlo methods.

For the differential cross sections in the subsequent sections an error of 10% due to the procedure used to determine the inclusive D meson yields per bin is added quadratically to the systematic uncertainties.

The uncertainty of the single track reconstruction efficiency are investigated as described in ref. [38].

6.1.2 Model Dependent Uncertainties

Various sources of model dependent uncertainties of the cross sections have been investigated and are summarized in Tab. 5. They are based on estimated errors on the total efficiency due to the uncertainties in the charm fragmentation function and its QCD evolution, in the gluon density of the proton, and in the effect of the charm quark mass on the inclusive D cross section. In the case of the charm production cross section, they also include an error for the estimate of the correction factor ξ. The total model dependent error is obtained by adding the different contributions quadratically.

The influence of the charm fragmentation function on the cross section is checked by using different parameterizations [20, 39]. A change in the total efficiency of less than 1% is found. The effect of the QCD evolution is studied by shifting the mean $\langle x_D \rangle$ by 0.1 which corresponds roughly to the difference in the gluon radiation by changing W by more than one order of magnitude. This results in an uncertainty of 4%.

The sensitivity of the measured cross section on the parton density in the proton has been studied by using different parameterization. In addition to the MRSH, MRSA$'$, MRSD0$'$ and GRV-HO parameterizations also the gluon density resulting from the NLO QCD fit to the total F_2 measurement from H1 [15] has been used for efficiency calculations. Only small variations in the total efficiency are observed.

In order to investigate the influence of the charm quark mass the correction factors have been calculated by using the AROMA Monte Carlo program with $m_c =$ 1.3 GeV, 1.5 GeV, and 1.7 GeV. Again only small variations in the efficiency are observed.

6.2 Differential Cross Section

Figure 5 shows the normalized differential cross section $1/\sigma \ d\sigma/dp_t(D^0)$ for inclusive D^0 and for D^0 via D^{*+} production for 10 GeV^2 $<$ Q^2 $<$ 100 GeV^2 and $0.01 < y < 0.7$. The normalization is done with respect to the integrated cross section. Only statistical errors are shown. No source of systematic uncertainties is found which would introduce additional uncorrelated systematic errors. Good agreement between the normalized $p_t(D^0)$ spectra of the two analyses is observed[8]. The data are also compared with the expectation from the boson gluon fusion process for charm quark masses of $m_c = 1.3$ GeV and $m_c = 1.7$ GeV. The measured differential distributions are in good agreement with the expectation. The differences due to the choice of the charm quark mass are much smaller than the present accuracy of the data. The data have also been compared to calculations using the GRV-HO [9] and MRSD0$'$ [10] gluon densities, which lead to normalized $p_t(D^0)$ distributions nearly identical with the one obtained for the MRSH parameterization.

[8]Although the D^0 produced via D^{*+} decay does not originate directly from the charmed quark, no differences between the $p_t(D^0)$ spectra for the two analyses are expected due the smallness of the kinetic energy available in the $D^{*+} \to D^0\pi^+$ decay.

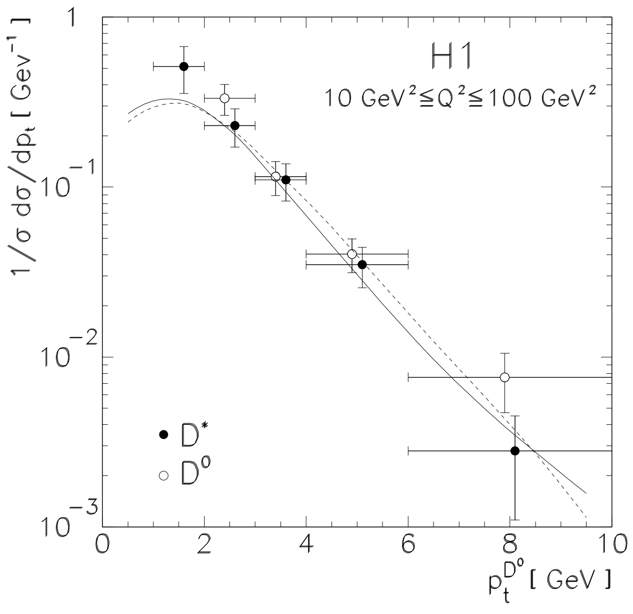

Figure 5: Normalized distributions of $1/\sigma\ d\sigma/dp_t(D^0)$ of the D^0 mesons from the D^{*+} (full points) and the D^0 analysis (open circles) in comparison to the AROMA expectation for $m_c = 1.3$ GeV (full line) and $m_c = 1.7$ GeV (dashed line) using the MRSH parameterization of the parton densities in the proton.

6.3 Mechanisms of Charm Production in ep Scattering

The charm production mechanisms in ep-scattering can be investigated by comparing fully corrected data with expectations for charm production off a charm quark in the proton sea and via boson gluon fusion (BGF). It is assumed that the fragmentation function $D_D^c(z)$ with $z = E_D/E_c$, the ratio of the charmed meson energy E_D to the charm quark energy E_c, is a universal function independent of the charm creation mechanism. This has been shown in ref. [40] to hold for both electron positron annihilation and neutrino-nucleon scattering [41, 42] provided the data is corrected for QCD radiation [8]. Figure 6 shows the corrected distributions $1/\sigma\ d\sigma/dx_D$, which are a convolution of the charm production spectrum with the fragmentation function in comparison with:

1. Monte Carlo simulated data using the AROMA generator in which charmed quarks are produced by BGF and fragmented according to JETSET.

2. Measurements of $\overset{(-)}{\nu} N$-scattering by the CDHS [41] and E531 [42] experiments, where charm production is expected to proceed mainly via $W^{\pm}$-scattering off a strange sea quark in the proton[9] (in analogy to Fig. 1a). It can be shown that the variable z, measured in the proton rest frame, approximately transforms

[9]In case of the νN scattering, the data also include sizeable contributions from valence quarks.

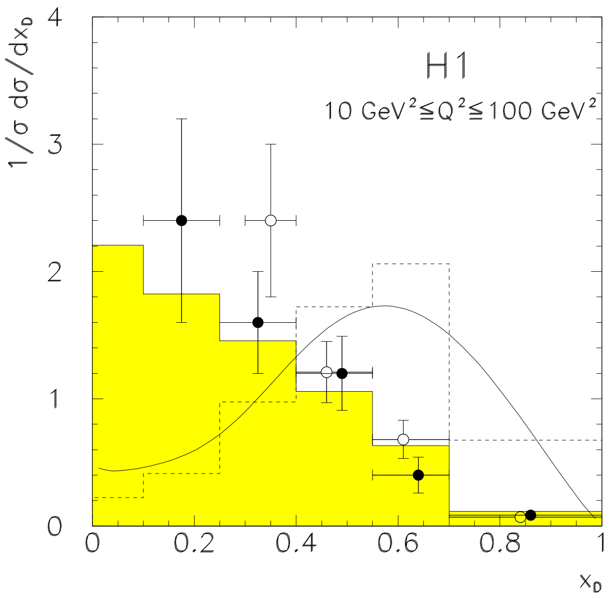

Figure 6: Normalized x_D distribution in deep inelastic ep scattering at $\langle W \rangle \approx 125$ GeV for $|\eta_D| < 1.5$. The open points represent the D^0 data, the closed points the D^* data. The shaded histogram shows the expectation of the boson gluon fusion process according to the AROMA Monte Carlo simulation. The dashed histogram shows the expectation from a charm sea contribution, calculated by selecting QPM events with the LEPTO/MEPS Monte Carlo program. The full line gives the result of the QCD evolution of the $\overset{(-)}{\nu} N$ data.

into x_D in the W^*p system. The results are evolved from $\langle W \rangle = 8$ GeV to $\langle W \rangle = 125$ GeV [8].

3. Monte Carlo simulated data using the LEPTO 6.1 generator, from which only charm sea quark events are selected. The fragmentation is modelled using JETSET.

The data are restricted to the region $|\eta_D| < 1.5$ in order to avoid large x_D dependent correction factors due to the detector acceptance. The total error is obtained by adding in quadrature the statistical error for the real and simulated data and the sum of the model dependent systematic uncertainties. The measurement errors are dominated by statistical effects. No source of systematic uncertainties is found which would introduce significant uncorrelated errors. Good agreement is observed between the x_D distribution obtained from the two different analyses.

The differences between the expectation from the BGF model, where two charm quarks are recoiling against the proton remnant in the hadronic center of mass system, on the one hand and the predictions from the $\overset{(-)}{\nu} N$ data and the quark parton model, where only one charm quark emerges opposite to the proton remnant, on the other hand are

Mode	$\langle Q^2 \rangle$ [GeV]	$\langle x \rangle$	$F_2^{c\bar{c}}$	$F_2^{c\bar{c}}/F_2$
D^*	12	.0008	$0.211 \pm 0.049\ ^{+0.045}_{-0.040}$	$0.198 \pm 0.045\ ^{+0.039}_{-0.033}$
D^0	12	.0020	$0.263 \pm 0.036\ ^{+0.043}_{-0.041}$	$0.304 \pm 0.043\ ^{+0.045}_{-0.042}$
D^*	12	.0032	$0.190 \pm 0.054\ ^{+0.052}_{-0.049}$	$0.254 \pm 0.072\ ^{+0.063}_{-0.058}$
D^*	25	.0008	$0.324 \pm 0.099\ ^{+0.065}_{-0.058}$	$0.244 \pm 0.075\ ^{+0.044}_{-0.038}$
D^0	25	.0020	$0.253 \pm 0.069\ ^{+0.041}_{-0.040}$	$0.248 \pm 0.086\ ^{+0.035}_{-0.033}$
D^*	25	.0032	$0.222 \pm 0.066\ ^{+0.044}_{-0.039}$	$0.255 \pm 0.076\ ^{+0.045}_{-0.038}$
D^*	45	.0020	$0.156 \pm 0.070\ ^{+0.031}_{-0.028}$	$0.127 \pm 0.059\ ^{+0.023}_{-0.020}$
D^0	45	.0032	$0.275 \pm 0.074\ ^{+0.045}_{-0.042}$	$0.249 \pm 0.071\ ^{+0.035}_{-0.033}$
D^*	45	.0080	$0.200 \pm 0.064\ ^{+0.040}_{-0.035}$	$0.269 \pm 0.088\ ^{+0.047}_{-0.039}$

Table 6: The value of $F_2^{c\bar{c}}$ and of the ratio $F_2^{c\bar{c}}/F_2$. The errors refer to the statistical and the experimental systematic errors.

evident. The BGF model agrees very well with the data which justifies the usage of this model throughout the paper.

To determine the fraction of the charm production cross section which may be attributed to a photon scattering off charm sea quarks in the proton, a superposition of the boson gluon fusion and the sea quark predictions, i.e. a function of the shape

$$1/\sigma d\sigma/dx_D = (1-\epsilon)(1/\sigma d\sigma/dx_D)_{BGF} + \epsilon(1/\sigma d\sigma/dx_D)_{sea} \tag{13}$$

is fitted to the x_D distribution of Fig. 6. Depending on the form of a charm sea quark contribution, i.e. using the results of the LEPTO Monte Carlo generator or the $\overset{(-)}{\nu} N$ data, and depending on the charm quark mass m_c, the fit yields values for ϵ between -0.062 ± 0.035 and -0.041 ± 0.031. According to the Bayesian approach [23] these values are converted to an upper limit on a charm sea quark contribution to charm production in deep inelastic ep scattering in the kinematic range at HERA of

$$\epsilon < 0.05 \tag{14}$$

at the 95% confidence level. It may thus be assumed that boson gluon fusion is the dominant charm production process in DIS at HERA.

6.4 Charm Contribution to the Proton Structure Function

The charm contribution $F_2^{c\bar{c}}(x, Q^2)$ to the structure function is obtained by using the expression for the one photon exchange cross section for charm production

$$\frac{d^2\sigma^{c\bar{c}}}{dxdQ^2} = \frac{2\pi\alpha^2}{Q^4 x}\left(1+(1-y)^2\right)\ F_2^{c\bar{c}}(x, Q^2)\ , \tag{15}$$

Systematic Errors on $F_2^{c\bar{c}}$	D^0	D^{*+}
fit	0.14	0.15
track efficiency	$^{+0.06}_{-0.02}$	$^{+0.09}_{-0.03}$
bin migrations	0.02	0.05
luminosity	0.015	0.015
γp contribution	<0.004	<0.004
radiative corrections	0.03	0.03
fragmentation gluon splitting	0.02	0.02
b contribution	<0.02	<0.02
charm fragmentation function	0.04	0.04
$P(c \to D)$	0.05	0.07
total	$^{+0.17}_{-0.16}$	$^{+0.20}_{-0.19}$

Table 7: Summary of the average relative systematic uncertainties on the measurement of $F_2^{c\bar{c}}$.

with the simplification that the Callan-Gross relation holds, i.e. $R = F_2/2xF_1 - 1 = 0$. According to QCD calculations a maximum value of $R \approx 0.38$ is expected in the kinematic range explored in the present analysis. An increase in $F_2^{c\bar{c}}(x, Q^2)$ of at most 2% is obtained at small x for $R = 1$.

The charm contribution to the proton structure function is obtained from the numbers of reconstructed D^{*+} and D^0 mesons, which are converted to bin averaged cross sections according to Eqns. (11,12) and using the Monte Carlo efficiency calculation. The coarse binning in x and Q^2 is dictated by the small statistics available. The bin averaged cross section is corrected for QED radiative effects using the program HECTOR [31].

In Tab. 6 the results of the $F_2^{c\bar{c}}$ measurements are summarized. The errors refer to the statistical and to the experimental systematic uncertainties. The systematic uncertainties are summarized in Tab. 7. They include an error due to the angular and energy resolution of the electron measurement, which is dominated by the uncertainty of the BEMC energy calibration. A shift in the energy scale of 1% introduces uncertainties of 6% (9%) in $F_2^{c\bar{c}}$ for the low (high) x bin in the D^{*+} analysis at $\langle Q^2 \rangle = 12$ GeV^2 due to bin migrations in x. For all other bins this effect is below 5%. The experimental systematic errors also include the uncertainties in the determination of $P(c \to D^{*+})$ and $P(c \to D^0)$.

The measurement of $F_2^{c\bar{c}}$ is found to be fairly insensitive to the actual choice of the parameterization of the gluon density in the proton. Using GRV-HO or MRSD0$'$ parameterization of the parton densities instead of MRSH , changes the result by less

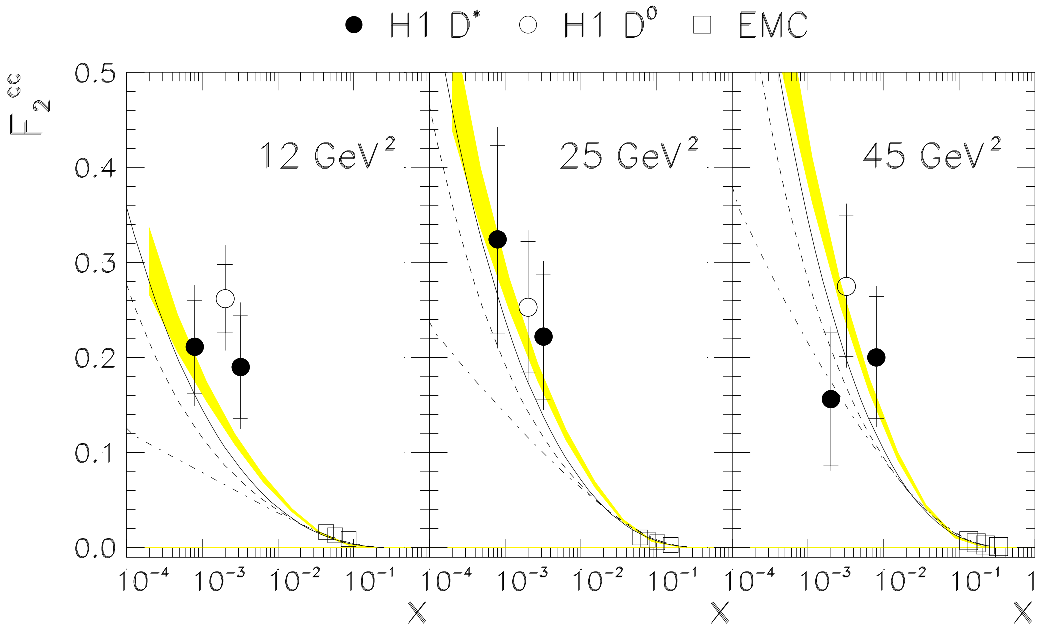

Figure 7: The charm contribution $F_2^{c\bar{c}}$ to the proton structure function as derived from the inclusive D^{*+} (full dots) and D^0 analysis (open circles) in comparison with the NLO calculations based on GRV-HO (full line), MRSH (dashed line), and MRSD0′ (dash-dotted line) parton distributions using a charm quark mass of $m_c = 1.5$ GeV for $\langle Q^2 \rangle = 12,\ 25$ and45 GeV^2. The inner (outer) error bars refer to the statistical (total) errors. The shaded band represents the prediction from the H1 NLO fit to the F_2 measurements. The EMC data are also shown (open boxes).

than 2% and 5%, respectively.

Table 6 also includes the ratio $F_2^{c\bar{c}}/F_2$ where the $F_2(x, Q^2)$ measurement is taken from ref. [15]. Within the accuracy of the charm data this ratio seems to be constant in the kinematic range explored in the current analysis. In particular the steep rise of $F_2^{c\bar{c}}/F_2$ with Q^2 for fixed x, as found by the EMC experiment [2] at considerably larger x, is not observed at HERA. The average yields

$$\left\langle F_2^{c\bar{c}}/F_2 \right\rangle = 0.237 \pm 0.021 \begin{array}{c} +0.043 \\ -0.039 \end{array}, \tag{16}$$

which is an increase of about one order of magnitude of the overall charm contribution compared to the EMC result. This is consistent with the measured rise of the gluon distribution towards low x and the dominance of the BGF process observed here. The present result on $F_2^{c\bar{c}}/F_2$ is also found to be in range predicted by ref. [43].

The $F_2^{c\bar{c}}$ measurements are displayed in Fig. 7 together with the result of the EMC collaboration [2]. The measurement at HERA extends the range of the $F_2^{c\bar{c}}$ measurement by two orders of magnitude towards smaller x values. The comparison of the H1 and EMC measurements reveals a steep rise of $F_2^{c\bar{c}}$ with decreasing x. The data is compared with NLO calculations [3] using the GRV-HO, the MRSH, and the MRSD0′ parameterizations of the gluon density in the proton for a charm quark mass $m_c = 1.5$ GeV. So far no experimental information is available on the gluon density in the proton observed in charm production at small x. Therefore, also the MRSD0′

parameterization is considered here, although it has already been excluded by inclusive measurements at HERA [44]. This parameterization also fails to describe $F_2^{c\bar{c}}$. The data lie systematically above all predictions which is to be expected from the measurement of the charm production cross section.

The data are also compared to the prediction from the H1 QCD fit to the F_2 measurements using a charm quark mass of $m_c = 1.5$ GeV. The error band shown for this fit includes the propagation of the statistical and the uncorrelated systematic errors on the total F_2 data through the fitting procedure. This prediction is systematically above all other calculations, independently of x and Q^2 but agrees better with the $F_2^{c\bar{c}}$ measurement. The charm data indicate a small excess of the measured $F_2^{c\bar{c}}$ with respect to all predictions in the lowest Q^2 bin.

The dominant uncertainty in the QCD calculations arises from the uncertainty in the charm quark mass. This affects mainly the lowest Q^2 bin, for which a variation of m_c by 200 MeV will change the prediction for $F_2^{c\bar{c}}$ by 15%. However, the measurement of $F_2^{c\bar{c}}$ shows the same m_c dependence. Therefore the comparison of the data with QcD calculations based on different gluon densities in the proton is nearly independent on the assumption made for the charm quark mass.

7 Conclusions

Results on inclusive D^0 and D^{*+} meson production in neutral current deep inelastic ep scattering at HERA have been presented. It has been shown, that the production dynamics of charmed mesons in the current and central fragmentation region may be described by the boson gluon fusion process.

The observed inclusive cross section ratio $\sigma(ep \to D^{*+}X)/\sigma(ep \to D^0X)$ is consistent with the results from e^+e^- and hadroproduction data.

From the inclusive D^0 and D^{*+} cross sections a charm production cross section in deep inelastic ep scattering for 10 GeV$^2 < Q^2 <$ 100 GeV^2 and $0.01 \leq y \leq 0.7$ of $\sigma\,(ep \to c\bar{c}X) = (17.4 \pm 1.6 \pm 1.7 \pm 1.4)$ nb has been derived. The data have been compared to different NLO calculations including the H1 QCD fit to the total F_2 data. The charm production cross section is found to be larger than predicted.

A first measurement of the charm contribution $F_2^{c\bar{c}}(x, Q^2)$ to the proton structure function for Bjorken x between $8 \cdot 10^{-4}$ and $8 \cdot 10^{-3}$ has been performed. Comparison of the present result with the EMC data reveals a steep rise of $F_2^{c\bar{c}}(x, Q^2)$ with decreasing x. Agreement is observed between the measured $F_2^{c\bar{c}}$ and the result of the NLO QCD fit of H1 to the inclusive F_2 data. Averaged over the kinematic range a ratio $\left\langle F_2^{c\bar{c}}/F_2 \right\rangle = 0.237 \pm 0.021\ ^{+0.043}_{-0.039}$ is obtained, which is one order of magnitude larger than at larger x.

Acknowledgments

We gratefully acknowledge the efforts of the HERA machine group, the DESY computer center, and the DESY directorate for their support. The non-DESY members of the collaboration wish to thank the DESY directorate for the hospitality extended to them while working at DESY. We would like to thank T. Behnke and M. Elsing for helpful discussions on the heavy flavor results from LEP and A. Vogt for fruitful discussions on charm production at HERA.

References

[1] A. Ali *et al.*, Proc. of the HERA Workshop, DESY, Hamburg, Vol. 1 (1988), 393; A. Ali and D. Wyler, Proc. of the Workshop "Physics at HERA", DESY, Hamburg, Vol. 2 (1991), 667 (and references therein); M.A.G. Aivazis *et al.*, Phys. Rev. D50 (1994) 3085; Phys. Rev. D50 (1994) 3102.

[2] EMC Collaboration, J.J. Aubert *et al.,* Nucl. Phys. B213 (1983) 31.

[3] E. Laenen *et al.*, Nucl. Phys. B392 (1993) 162, 229; E. Laenen *et al.*, Phys. Lett. B291 (1992) 325; S. Riemersma, J. Smith, and W.L. van Neerven, Phys. Lett. B347 (1995) 143.

[4] M.L. Mangano and P. Nason, Phys. Lett B285 (1992) 160; M. H. Seymour, Z. Phys. C 63 (1994) 99, Nucl. Phys. B436 (1995) 16.

[5] OPAL Collaboration, R. Akers *et al.*, Z. Phys. C67 (1995) 27.

[6] OPAL Collaboration, R. Akers *et al.*, Phys. Lett. B353 (1995) 595.

[7] S.J. Brodsky *et al.*, Phys. Lett. 93B (1980) 451; Phys. Rev. D 23 (1981) 2745; Phys. Rev. D52 (1995) 6285; G.A. Schuler, Nucl.Phys. B299 (1988) 21; G. Ingelman, L. Jönsson, and M. Nyberg, Phys. Rev. D47 (1993) 4872; G. Ingelman and M. Thunman, HEP-PH/9604289.

[8] G. Altarelli, Phys. Rep. 81 (1982) 1.

[9] M. Glück, E. Reya, and A. Vogt, Z. Phys. C 53 (1992) 127.

[10] A.D. Martin, R.G. Roberts, and W.J. Stirling, Phys.Lett. B306 (1993), 145.

[11] A.D. Martin, W.J. Stirling, and R.G. Roberts, Phys. Rev. D50 (1994) 6743.

[12] A.D. Martin, R.G. Roberts, and W.J. Stirling, Phys. Rev. D50 (1994) 6734.

[13] H1 Collaboration, I. Abt *et al.*, "The H1 Detector at HERA", DESY preprint, DESY H1-96-01 (1996), to be submitted to Nucl. Inst. Meth.

[14] H1 BEMC Group, J. Bán *et al.*, Nucl. Inst. and Meth. A 372 (1996) 399.

[15] H1 Collaboration, S. Aid *et al.*, Nucl. Phys. B470 (1996) 3.

[16] G. Ingelman, J. Rathsman, and G.A. Schuler, DESY preprint, DESY 96-058, and HEP-PH/9605285.

[17] M. Bengtsson, and T. Sjöstrand, Z. Phys. C37 (1988) 465; M. Bengtsson, G. Ingelman, and T. Sjöstrand, Proc. of HERA Workshop 1987, Ed. R.D. Peccei, DESY Hamburg 1988.

[18] G. Ingelman, "LEPTO version 6.1 - The Lund Monte Carlo for Deep Inelastic Lepton-Nucleon Scattering", TSL/ISV-92-0065.

[19] T. Sjöstrand, "PYTHIA 5.7 and JETSET 7.4 Physics and Manual", CERN-TH.7112/93.

[20] B. Anderson, G. Gustafson, and B. Söderberg, Z. Phys. C20 (1983) 317; M.G. Bowler, Z. Phys. C11 (1981) 169; D.A. Morris, Nucl. Phys. B313 (1989) 634.

[21] H1 Collaboration, T. Ahmed *et al.*, Nucl. Phys. B493 (1995) 471.

[22] G. Feldmann *et al.*, Phys. Rev. Lett. 38 (1977) 1313.

[23] Particle Data Group, M.Aguilar-Benitez *et al.*, Phys. Rev. D50 (1994).

[24] ARGUS Collaboration, H. Albrecht *et al.*, Z. Phys. C 52 (1991) 353.

[25] CLEO Collaboration, D. Bortoletto *et al.*, Phys. Rev. D 37 (1988) 1719.

[26] HRS Collaboration, P. Baringer *et al.*, Phys. Lett. B206 (1988) 551.

[27] DELPHI Collaboration, P. Abreu *et al.*, Z. Phys. C 59 (1993) 533.

[28] ALEPH Collaboration, D. Buskulic *et al.*, Z. Phys. C 62 (1994) 1.

[29] NA32 Collaboration, S. Barlag *et al.*, Z. Phys. C 49 (1991) 555.

[30] E769 Collaboration, G.A. Alves *et al.*, Fermilab preprint, FERMILAB Pub-96/083, submitted to Phys. Rev. Lett.

[31] A. Arbuzov *et al.*, Comp. Phys. Comm. 94 (1996) 128.

[32] M. Glück, E. Hoffmann and E. Reya, Z. Phys. C13 (1982) 119.

[33] M. Glück, E. Reya and M. Stratmann, Nucl. Phys. B422 (1994) 37.

[34] M. Virchaux and A. Milsztajn, Phys. Lett. B274 (1992) 221.

[35] BCDMS Collaboration, A.C. Benvenuti *et al.*, Phys. Lett. B223 (1989) 485; CERN preprint CERN-EP/89-06.

[36] NMC Collaboration, M. Arneodo *et al.*, Phys. Lett. B364 (1995) 107.

[37] C. Pascaud and F. Zomer, LAL preprint LAL/94-42.

[38] H1 Collaboration, S. Aid *et al.*, DESY Preprint, DESY 96-55, submitted to Nucl. Phys. B.

[39] V.G. Kartvelishvili, A.K. Likehoded and V.A. Petrov, Phys. Lett. B78 (1978) 615; C. Peterson *et al.*, Phys. Rev. D27 (183) 105; P. Collins and T. Spillar, J. Phys. G11 (1985) 1289.

[40] K. Kleinknecht and B. Renk, Z. Phys. C17 (1983) 325.

[41] CDHS Collaboration, H. Abramowic *et al.*, Z. Phys. C15 (1982) 19.

[42] E531 Collaboration, N. Ushida *et al.*, Phys. Lett. B206 (1988) 380.

[43] A.V. Kisselev and V.A. Petrov, CERN-TH/96-110.

[44] H1 Collaboration, I. Abt *et al.*, Nucl. Phys. B 407 (1993) 515.